Dalton Transactions

Accepted Manuscript

This article can be cited before page numbers have been issued, to do this please use: F. Liu, P. Tang, R. Ding, L. Liao, L. Wang, M. Wang and J. Wang, *Dalton Trans.*, 2017, DOI: 10.1039/C7DT01099K.

ROYAL SOCIETY OF CHEMISTRY

rsc.li/dalton

View Article Online
DOI: 10.1039/C7DT01099K

Journal Name

ARTICLE

A glycosylation strategy to develop low toxic naphthalimide fluorescent probe for the detection of Fe^{3+} in aqueous medium

Received 00th January 20xx,
Accepted 00th January 20xx

DOI: 10.1039/x0xx00000x

www.rsc.org/

Feiyang Liu,[a] Piaoping Tang,[a] Ruihua Ding,[a] Lujuan Liao,[a] Lisheng Wang,[a] Mian Wang*[b] and Jianyi Wang* [a,c]

A glycosylation strategy based on click chemistry was employed to develop naphthalimide-based Fe^{3+} fluorescent probe with low cytotoxicity and good water-solubility. The selectivity and sensitivity to Fe^{3+} of three synthesized naphthalimide-based fluorescent probes follows a **Nap-PZ**<**Nap-OH**<**Nap-Glc** trend, because **Nap-PZ** was modified by good water-soluble group. The cytotoxicity follows a **Nap-PZ**>**Nap-OH**>**Nap-Glc** trend, because the exposed toxic group of **Nap-PZ** was shielded by good biocompatible group. The detection limit toward Fe^{3+} ion follows a **Nap-PZ(**7.40×10^{-6}M**)**>**Nap-OH(**2.73×10^{-7}M)>**Nap-Glc**(4.27×10^{-8}M) trend. Moreover, Nap-Glc could be used to detect Fe^{3+} in living cells. The fluorescent "off-on" response of **Nap-Glc** towards Fe^{3+} could be recognized by naked-eye, and the "off-on" fluorescent mechanism was demonstrated by theoretical calculations. Therefore, **Nap-Glc** was a novel glucosyl naphthalimide fluorescent probe for environmental or biological detection of Fe^{3+} with low cytotoxicity and good water-solubility.

Introduction

Iron (especially Fe^{3+}) is the most abundant trace elements in human body and plays an essential role in various biochemical processes involving oxygen transport, exotic metabolism, DNA synthesis and repair[1]. The deficiency of iron would cause anemia, hemochromatosis, liver damage, diabetes and cancer[2,3], and the excess of iron could induce Alzheimer's, Huntington's, neurodegenerative diseases and Parkinson's diseases[4, 5] etc. Also, Fe^{3+} was important pollutant source of the environment. Therefore, the monitoring and detection of Fe^{3+} was very significant in both biosystem and environment.

Spectrophotometry, atomic absorption spectroscopy and voltammetry inductively coupled plasma mass spectroscopy were familiar method to detect Fe^{3+}. But high cost, time-consuming and sampling complexity limited wide application of these methods. The fluorescence probes towards Fe^{3+}, including rhodamine[6-8], fluorescein[9], thiazolo-pyrimidine[10], imidazole[11], naphthalimide[12] derivatives, recently drawn tremendous attention from academia and industrial circles because of their high efficiency, economy, convenience manipulation[13-15]. However, several shortcomings limited wide application of these probes towards Fe^{3+}: poor water-solubility[7,9-12], high toxicity[16-18], slow-response towards Fe^{3+} ions[6-8,11]. The fluorescent quenching caused by the paramagnetism of iron was another shortcoming[9]. Among these probes, naphthalimide was widely used as chemosensors monitoring metal ions[19-25], pH[26,27] and endogenous substances[28-34] because of its good photo-physical and chemical properties. The water-solubility and cytotoxicity of naphthalimide could was overcome by introducing a glycosyl group to the naphthalimide skeleton[35, 36], but this probe was mainly used to detect zinc ion rather than Fe^{3+} ion. To date, the glycosylation from click reaction[37-42] or glycosidic reaction[43-45] has emerged as a promising strategy for the modification of hydrophobic and toxic materials.

Therefore, in this work, our aim was to develop novel naphthalimide-based fluorescent probes towards Fe^{3+} with high efficient, good water-solubility and low cytotoxicity, and the obtained target compound (**Nap-PZ**, **Nap-OH** and **Nap-Glc**) was correspondingly characterized and evaluated.

Results and Discussion

Synthesis of Fe^{3+} fluorescent probes

As shown in Scheme 1, compound **Nap-PZ** was synthesized by conjugating 1, 8-naphthalimid with piperazine which acts as electron-donator and fluorescent quencher based on photo induced electron transfer (PET) effect. **Nap-PZ** was modified by a hydrophilic azole group to afford **Nap-OH**. A hydrophilic and biocompatible glucose unit was introduced to **Nap-PZ** through

[a] School of Chemistry and Chemical Engineering,Guangxi University, Nanning 530004, China. * email: jianyiwang@gxu.edu.cn
[b] College of Life Science and Technology, Guangxi University, Nanning530004, China.* email: mianwang23@163.com
[c] Guangxi Colleges and Universities Key Laboratory of Applied Chemistry Technology and Resource Development, Nanning 530004, China.

† Electronic Supplementary Information (ESI) available: [absorption spectra of **Nap-PZ, Nap-OH** and **Nap-Glc** towards metal ions; Fluorescence concentration titration spectra and titration curves of **Nap-PZ** and **Nap-OH**; Acid-base titration experiments of **Nap-Glc**; ESI-MS spectrum of Nap-Glc-Fe^{3+};theoretical calculations of **Nap-Glc** and **Nap-Glc-Fe^{3+}** complex; Experimental procedures of compound **3**,**5**,**6**;$^{1}H/^{13}C$ NMR of all compounds; HRMS spectra of three probes]. See DOI: 10.1039/x0xx00000x

View Article Online
DOI: 10.1039/C7DT01099K

click reaction to afford **Nap-Glc**. The structures of the targeted compounds were confirmed by ^{1}H NMR, ^{13}C NMR, and HRMS.

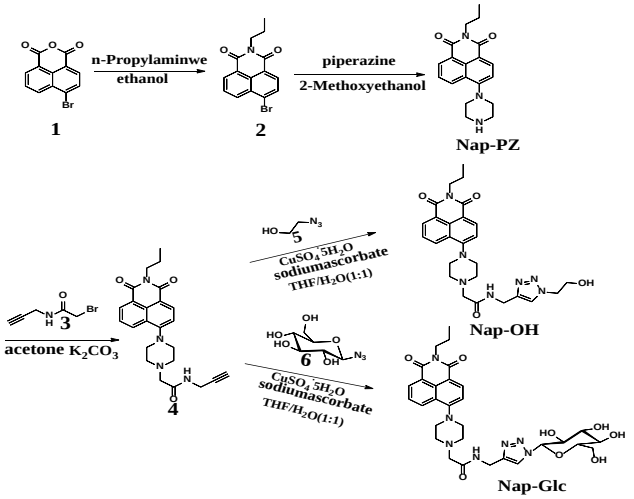

Scheme 1 Synthetic routes of **Nap-PZ**, **Nap-OH** and **Nap-OH**

Selectivity of Nap-PZ, Nap-OH and Nap-Glc for Fe^{3+} ion

To evaluate selectivity of **Nap-PZ**, **Nap-OH** and **Nap-Glc** (Fig. 1a) towards Fe^{3+}, the fluorescence spectra of **Nap-OH** and **Nap-Glc** could be directly measured in phosphate buffer (pH=6.50) medium, whereas **Nap-PZ** required a mixed medium with 10% ethanol. As shown in Fig.1b, **Nap-PZ** presented a strong background fluorescence, which could be attributed to protonation of aqueous medium to the piperazine nitrogen of **Nap-PZ**, inhibiting PET effect of naphthalimide. And **Nap-PZ** almost responded to all these metal ions, being difficult to distinguish Fe^{3+} from other metal ions. When a hydrophilic azole group was introduced to **Nap-PZ** to afford **Nap-OH**, the background fluorescence disappeared, because the exposed piperazine nitrogen of **Nap-PZ** was shielded. Upon addition of Fe^{3+}, the **Nap-OH** solution exhibited a clear fluorescent enhancement (Fig. 1c) at 528 nm. While the addition of other metal ions(Ce^{3+}, Eu^{3+}, Ba^{2+}, Ca^{2+}, Cd^{2+}, Co^{2+}, Fe^{2+}, Mg^{2+}, Mn^{2+}, Ni^{2+}, Pb^{2+}, Zn^{2+},Ag^{+}, K^{+}, Li^{+}, Na^{+}, NH_4^{+}), the **Nap-OH** solution only showed small fluorescent enhancement, although **Nap-OH** was slightly disturbed Pb^{2+}. When a better hydrophilic glucose unit was introduced through click reaction to form **Nap-Glc**, the **Nap-Glc** solution exhibited a remarkable fluorescent enhancement (Fig. 1d) at 528 nm toward Fe^{3+} ion compared with other metal ion. Similar phenomenon could be observed in absorption spectra of these probes (Fig. S1). Under the irradiation of ultraviolet lamp(365 nm), one could hardly distinguish the **Nap-PZ-Fe^{3+}** solution from **Nap-PZ**-other ions solution by naked-eye, and the **Nap-PZ** solution was "lighted up" by all metal ions(the first row). Comparatively, **Nap-OH** and **Nap-Glc** could easily recognized Fe^{3+} rather than other metal ions (Fig.1e). The reason should be attributed to the water-solubility of **Nap-OH** and **Nap-Glc** over **Nap-PZ**. In addition, the fluorescence of **Nap-OH** and **Nap-Glc** could be quenched upon titration with Cu^{2+}, which was caused by the well-known paramagnetic effect of Cu^{2+} ion[23, 46], Therefore, the **Nap-OH** and **Nap-Glc** probes with good soluble group showed better selectivity for Fe^{3+} than **Nap-PZ**.

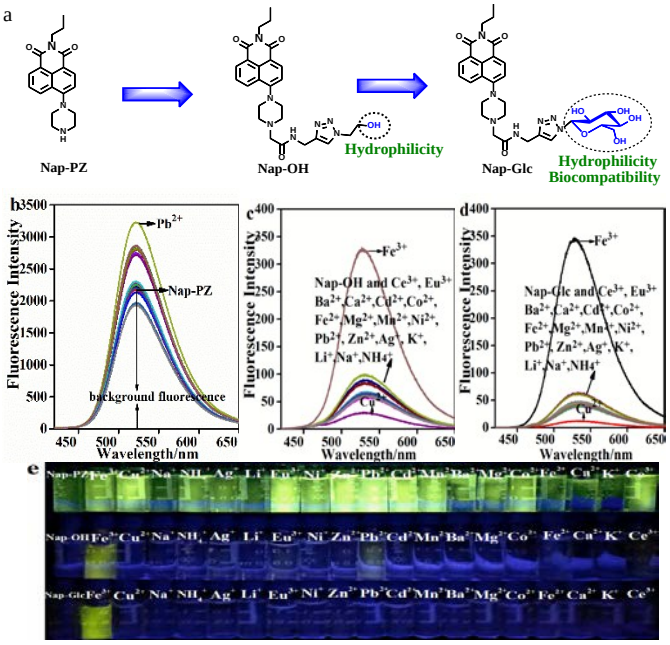

Fig.1(a) Structure of **Nap-PZ**, **Nap-OH** and **Nap-Glc**. The Fluorescence spectra of **Nap-PZ** (b), **Nap-OH** (c) and **Nap-Glc** (d) (10 μM) upon addition of 5 equiv different metal cations. (e) The color changes of three probes in the presence of different metal cations under UV light (365 nm).

Sensitivity of Nap-PZ, Nap-OH and Nap-Glc for Fe^{3+} ion

To assess the sensitivity of these probes toward Fe^{3+}, titration experiments were carried out in phosphate buffer (pH=6.50). The fluorescence intensity of **Nap-Glc** solution (Fig. 2) at 528 nm was substantially increased when Fe^{3+} ions was gradually added (0–50 mM), which was linear with the concentration of Fe^{3+} ions in the range of 0 to 20 mM. The detection limit of **Nap-Glc** toward Fe^{3+} ion was calculated to be 4.27×10^{-8}M, while the detection limit was 7.40 $\times 10^{-6}$ M for **Nap-PZ** (Fig .S2) and 2.73 $\times 10^{-7}$ M for **Nap-OH** (Fig .S3), respectively. The detection limit was calculated by the formula 3δ/k, where k is the slope between fluorescent intensity versus sample concentration, and δ represents the standard deviation obtained by maximal fluorescence intensity of free probes. The outstanding detection level of **Nap-Glc** could be ascribed to their good water-solubility compared with **Nap-PZ**.

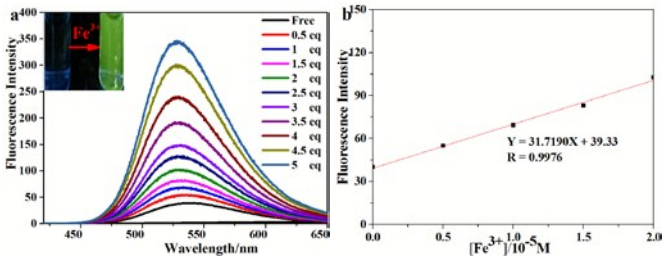

Fig.2 (a) Fluorescence changes of **Nap-Glc** (10 μM) in phosphate buffer (pH=6.50) with 0-5 equiv Fe^{3+}.Inset: The color changes of **Nap-Glc** in the presence of 5 equiv Fe^{3+} under UV light of 365 nm. (b) Plots of fluorescence intensity as a function of Fe^{3+} concentrations from 0– 20 μM.

Cytotoxicity assays

Low toxicity is another requirement for the application of probes in biosystem or environment. As shown in Fig. 3, **Nap-PZ** displayed an obvious concentration-dependent toxicity towards HepG2 cell and nearly killed all cells at a concentration of 80μM. When a hydrophilic azole group was introduced to **Nap-PZ**, **Nap-OH** showed much less toxic than **Nap-PZ**. The main reason was that the exposed piperazine nitrogen of **Nap-PZ**, which might be a toxic group, was shielded by a biocompatible azole group. When this exposed piperazine nitrogen of **Nap-PZ** was modified by a better biocompatible glycosyl moiety (a nutrient group), **Nap-Glc** hardly showed toxic towards HepG2 cell in a wide range of concentrations, was even favorable for growth of HepG2 cell. Therefore, non-toxic **Nap-Glc** could well satisfy the detection of Fe^{3+} in vitro or vivo.

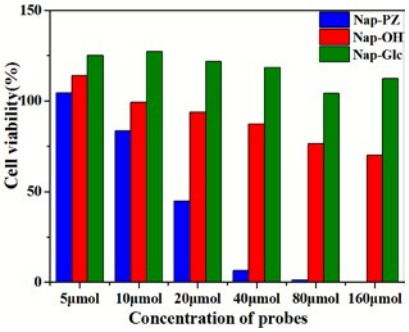

Fig. 3 Cell viability of HepG2 treated with different concentrations of **Nap-PZ**, **Nap-OH** and **Nap-Glc**.

Practical application of Nap-Glc

Since probe **Nap-Glc** with low cytotoxicity possessed desired selectivity and sensitivity toward Fe^{3+}, good competition, short response time and wide working pH rang were also necessary for practical application of probes. When Ag^{+}, Ba^{2+}, Ca^{2+}, NH_4^{+}, Cd^{2+}, Co^{2+}, Cu^{2+}, K^{+}, Li^{+}, Mg^{2+}, Mn^{2+},Na^{+}, Ni^{2+}, Zn^{2+}, Ce^{3+}, Eu^{3+}, Fe^{2+}, Pb^{2+} were added into the **Nap-Glc** solution (10 μM), no significant fluorescent enhancement were observed at 528 nm (black bars), and the fluorescent intensity was dramatically enhanced when Fe^{3+} was added into the **Nap-Glc** solution with other competitive metal ions (red bars) (Fig. 4). Similarly, **Nap-Glc** hardly responded to the anions Br^{-}, CH_3COO^{-}, Cl^{-}, F^{-}, $H_2PO_4^{2-}$, HSO_3^{-}, I^{-}, NO_3^{-}, $S_2O_3^{2-}$, SO_4^{2-} etc, and the addition of Fe^{3+} into the **Nap-Glc** solution with these anions caused dramatic enhancement of the fluorescence (Fig. 5). Therefore, **Nap-Glc** had an excellent anti-disturbance capacity, could be independently applied for the detection of Fe^{3+} in aqueous medium, and not disturbed by the ions listed above.

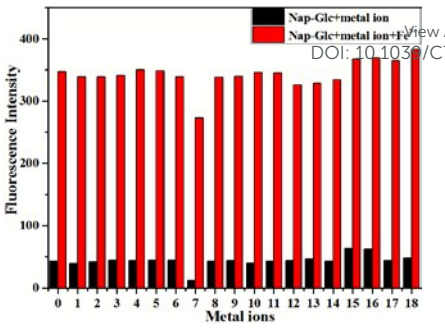

Fig.4 The fluorescence intensity (528 nm) of **Nap-Glc** (10 μM)toward Fe^{3+} with other ions: 0, no ion; 1, Ag^{+};2, Ba^{2+}; 3, Ca^{2+}; 4, NH_4^{+}; 5, Cd^{2+};6, Co^{2+}; 7, Cu^{2+}, 8, K^{+}; 9, Li^{+}; 10, Mg^{2+};11, Mn^{2+}; 12, Na^{+}; 13, Ni^{2+}; 14, Zn^{+}; 15 Ce^{3+}; 16, Eu^{3+}; 17, Fe^{2+}; 18, Pb^{2+}.

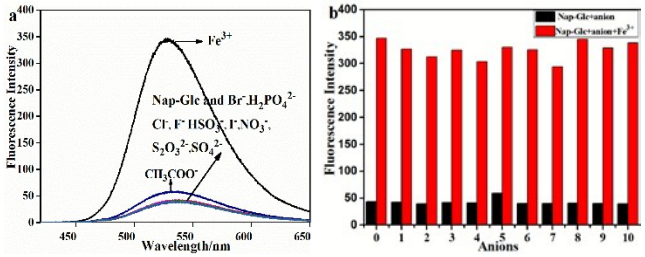

Fig.5 (a) Fluorescence changes of **Nap-Glc** in the presence of different anions. (b) The fluorescence intensity (528 nm) of **Nap-Glc** (10 μM) toward Fe^{3+} upon addition of 0, no anions; 1, Br-;2, CH_3COO^{-}; 3, Cl^{-}; 4, F^{-}; 5, $H_2PO_4^{2-}$, 6, HSO_3^{-}; 7, I^{-}; 8, NO_3^{-};9, $S_2O_3^{2-}$; 10, SO_4^{2-}.

As shown in Fig.6, when 5 equiv. Fe^{3+} was added, the fluorescence of **Nap-Glc** in phosphate buffer (pH=6.50) instantly enhanced and reached the maximum within one minute. Furthermore, the fluorescence intensity of the **Nap-Glc** solution with Fe^{3+} ions was kept steady in the following 30 minutes. So short-response time of **Nap-Glc** toward Fe^{3+} could well satisfy the requirement of real-time and quick detection.

The acid-base titration experiments (Fig.S4) showed that the working pH range for **Nap-Glc** detecting Fe^{3+} was about 4-8, where the fluorescent sensing behaviour was dominated by Fe^{3+}. No fluorescence could be observed in the range of pH>8, which should be ascribed to the hydrolysis of Fe^{3+}.

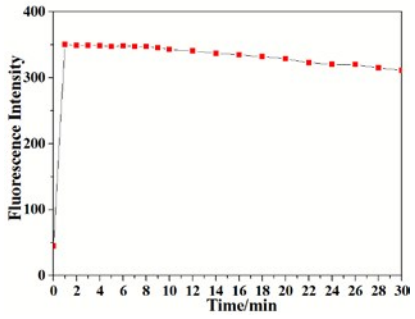

Fig.6 Time response of **Nap-Glc** (10 μM) towads 5 equiv Fe^{3+} in phosphate buffer (pH=6.50).

To explore the application of **Nap-Glc** in biosystem, the living cell imaging was conducted in HepG2 cells. As shown in

Fig. 7, no fluorescence was observed when the cells were only treated with **Nap-Glc** (10 μM) (Fig. 7a). However, obvious fluorescence enhancement could be observed (Fig. 7b, c) when the cells were treated with different concentrations of Fe^{3+} and **Nap-Glc** (10 μM), and the fluorescence intensity in HepG2 cells increased with the incremental concentrations of Fe^{3+}. Clearly, **Nap-Glc** showed good membrane-permeable and could be used to detect Fe^{3+} in biosystem.

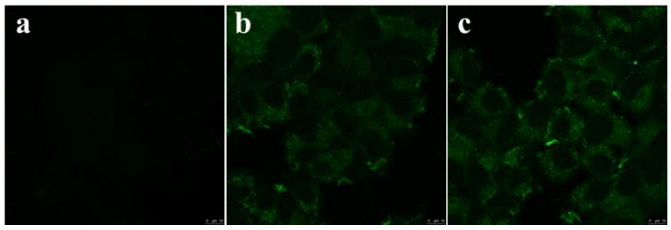

Fig.7 Confocal fluorescence microscopic images of HepG2 cells. (a) Cells treated with **Nap-Glc** (10 μM) alone; (b) Cells treated with **Nap-Glc** (10 μM) and Fe^{3+} (1 eq); (c) Cells treated with **Nap-Glc** (10 μM) and Fe^{3+} (10 eq).

Comparison of Nap-Glc with other Fe^{3+} fluorescent sensors.

The comparison of **Nap-Glc** and other Fe^{3+} fluorescence probe were summarized in Table1. We noticed that **Nap-Glc** exhibited high selectivity toward Fe^{3+} and was not disturbed by other metals ions, while the reported fluorescence sensors for Fe^{3+} usually were disturbed by other metals cations such as Cu^{2+} ion[47,51] and Hg^{2+} ion[48-50]. **Nap-Glc** showed excellent detection limit and very short response time compared with these sensors[3, 8, 11, 47, 48, 50, 51]. More important, **Nap-Glc** could be performed in 100% aqueous medium and most of reported Fe^{3+} sensors[9, 11, 12, 47-49] required a mixed medium of organic solvent and water. Also, **Nap-Glc** showed less toxic in higher dose range compared with the reported Fe^{3+} probes[11, 12, 50].

Table 1. Comparison of **Nap-Glc** with other reported Fe^{3+} fluorescent sensor.

Ref of sensor	Disturbed ions	Detection limit (M)	response time	media	toxic
3	no	4.5×10^{-6}	No discuss	Tris–HCl buffer	No discuss
8	no	1×10^{-7}	40 min	H_2O-CH_3CN (95:5=v/v)	No discuss
9	no	No discuss	No discuss	MOPS buffer	No discuss
11	no	1.2×10^{-7}	40 min	Potassium phosphate buffer acetone (1:4v/v)	No toxic at 5 μM
12	no	3.0×10^{-8}	< 1 min	Tris HCl–CH_3CN (1:1v/v 0.01M)	No toxic at 25 μM
47	Cu^{2+}	7.65×10^{-6}	No discuss	DMF	No discuss
48	Hg^{2+}	3.9×10^{-9}	30 mim	H_2O-C_2H_5OH (4:1,V/V)	No discuss
49	Hg^{2+}	2.72×10^{-8}	No discuss	CH_3CN-H_2O (v/v=3:7)	No discuss
50	Hg^{2+}	1.3×10^{-7}	> 60 min	H_2O–CH_3CN (9:1=v/v)	No toxic 6.25 μM
51	Cu^{2+}	2.2×10^{-6}	No discuss	H_2O-CH_3OH (v/v=9/1)	No discuss
Nap-Glc	no	4.27×10^{-8}	< 1 min	phosphate buffer	No toxic 160 μM

Stoichiometry and recognition mode of Nap-Glc toward Fe^{3+}

To explore the binding mode of **Nap-Glc** toward Fe^{3+}, Job's plot analysis was carried out with the total concentration of **Nap-Glc** and Fe^{3+} solution being constant, and the [**Nap-Glc**]/[**Nap-Glc+Fe^{3+}**] value varying from 0.1 to 0.9 (Fig.8). When [**Nap-Glc**]/[**Nap-Glc+Fe^{3+}**] value was about 1/3, the solution emitted the strongest fluorescence, suggesting that one equiv **Nap-Glc** was most likely to bind 2 equiv Fe^{3+} ion (1:2 stoichiometry). 1:2 stoichiometry of **Nap-Glc–Fe^{3+}** complex was also confirmed by ESI-MS spectrum data (Fig.S5). Among these two equiv Fe^{3+} ion, one equiv. Fe^{3+} bound to the piperazine nitrogen of **Nap-Glc**, inhibiting PET effect from electron-donator piperazine to electron-receptor 1, 8-naphthalimide moiety, recovered the strong fluorescence of 1, 8-naphthalimide, and another equiv. Fe^{3+} ion might bind to the glycosyl moiety[52, 53]. The recognition mechanism of **Nap-Glc** toward Fe^{3+} was thus proposed in Scheme 2.

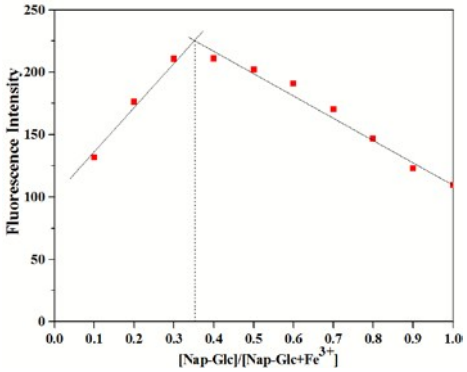

Fig. 8 Job's plot of **Nap-Glc** with Fe^{3+} (the total concentration of **Nap-Glc** and Fe^{3+} solution was 50 μM).

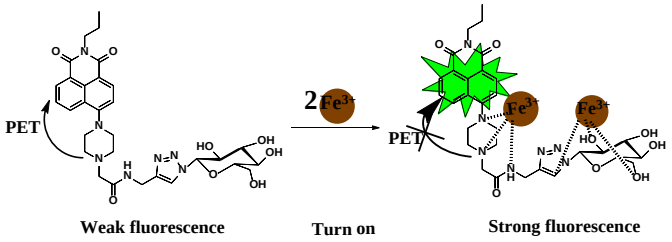

Scheme 2 Proposed "off-on" fluorescent mechanism of **Nap-Glc** towards Fe^{3+}.

Fluorescence mechanism reflected by theoretical calculations

To demonstrate "off-on" fluorescent mechanism of **Nap-Glc** toward Fe^{3+}, theoretical calculations were performed. When Fe^{3+} bound to the piperazine nitrogen of **Nap-Glc** and PET effect from piperazine to 1, 8-naphthalimide was inhibited, the LUMO-HOMO energy gap was calculated to reduce from 3.464 ev for **Nap-Glc** to 2.874 ev for **Nap-Glc-Fe^{3+}** complex(Fig.9),

resulting in "Fluorescence on" of **Nap-Glc**. The UV-spectrum was calculated to be around 409 nm with f=0.3326 for **Nap-Glc**(close to the experimental value 405 nm, Table S1), and about 376 nm for **Nap-Glc-Fe^{3+}** (close to the experiment value 385 nm, Table S2), also supporting that the calculated mechanism was credible. Further calculations on "Fluorescence on" mechanism of **Nap-Glc** were given in Figure S7.

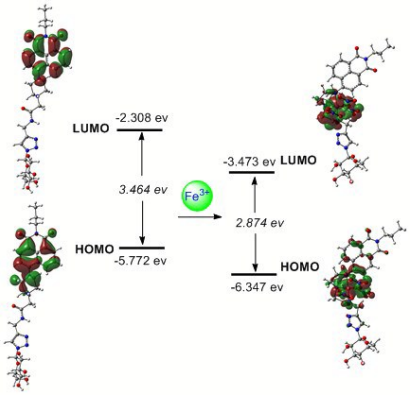

Fig. 9 "off-on" fluorescent mechanism of **Nap-Glc** given by theoretical calculations.

Conclusions

In this work, a glycosylation strategy based on click chemistry was employed to develop naphthalimide-based Fe^{3+} fluorescent probe with good water-solubility and low cytotoxicity. The selectivity and sensitivity to Fe^{3+} of three synthesized naphthalimide-based fluorescent probes follows a **Nap-PZ<Nap-OH<Nap-Glc** trend, where Nap-PZ was modified by good water-soluble group. The cytotoxicity to cell follows a **Nap-PZ>Nap-OH>Nap-Glc** trend. The reason was that the exposed piperazine nitrogen of Nap-PZ was shielded by good biocompatible group. The detection limit toward Fe^{3+} ion toward Fe^{3+} ion follows a **Nap-PZ** (7.40×10^{-6}M)>**Nap-OH** (2.73×10^{-7}M)>**Nap-Glc**(4.27×10^{-8}M) trend. The fluorescent "off-on" response of Nap-Glc at 528 nm (λex=405 nm) towards Fe^{3+} was easily recognized by naked-eye under UV light. Nap-Glc rapidly responded to Fe^{3+} within one minute. Thus, Nap-Glc was a novel glucosyl naphthalimide fluorescent probe with excellent water-solubility and low cytotoxicity, which could be independently applied for the detection of Fe^{3+} in aqueous medium, and not disturbed by Ag^{+}, Ba^{2+}, Ca^{2+}, NH_4^{+}, Cd^{2+}, Co^{2+}, Cu^{2+}, K^{+}, Li^{+}, Mg^{2+}, Mn^{2+},Na^{+}, Ni^{2+}, Zn^{2+}, Ce^{3+}, Eu^{3+}, Fe^{2+}, Pb^{2+} and Br^{-}, CH_3COO^{-}, Cl^{-}, F^{-}, $H_2PO_4^{2-}$, HSO_3^{-}, I^{-}, NO_3^{-}, $S_2O_3^{2-}$, SO_4^{2-} .1:2 stoichiometry was the most likely recognition mode of Nap-Glc toward Fe^{3+}, and the corresponding "off-on" fluorescent mechanism of Nap-Glc was demonstrated by theoretical calculations. The cell imaging assay indicated that Nap-Glc was membrane-permeable and could be used to detect Fe^{3+} in living cells.

Experimental

View Article Online
DOI: 10.1039/C7DT01099K

Materials and instruments

All regents were commercially available and used without further purification. ^{1}H NMR and ^{13}C NMR spectra were recorded on Bruker 600MHz at 25°C, TMS as the internal standard in $CDCl_3$, and solvent peak as the internal reference in CD_3OD. HRMS analysis was performed by Thermo Fisher Scientific LTQ FT Ultra. The UV-vis absorption and the fluorescence spectra were carried out by Shanghai JingHua 7600 UV visible spectrophotometer (dual beam) and Shimadzu RF-5301PC at room temperature, respectively. The cytotoxicity assays was conducted by ELX800 absorbance microplate reader. Cell image assays was performed by Multi-photon laser confocal scanning microscopy (LEICA-TCS-SP8MP).

Synthesis of the fluorescent probes

Synthesis of compound 2

As shown in Scheme 1, 4-Bromo-1, 8-naphthalic anhydride (0.8 g, 2.89 mmol) and n-Propylamine (0.262 ml, 3.18 mmol) were dissolved in ethanol (15 mL). The reaction mixture was stirred and refluxed for 4.5 h. After cooling to room temperature, the mixture was poured into ice water to form the precipitate. The precipitate was isolated, washed with water and cool ethanol, and then dried to afford grey white solid 2 (0.79 g; yield: 85.6%).^{1}H NMR (600 MHz, $CDCl_3$) δ 8.64 (d, J = 7.2 Hz, 1H), 8.54 (d, J = 8.4 Hz, 1H), 8.40 (d, J = 7.8 Hz, 1H), 8.03 (d, J = 7.8 Hz, 1H), 7.84 (t, J = 7.9 Hz, 1H), 4.23 – 4.03 (m, 2H), 1.84 – 1.67 (m, 2H), 1.03 (t, J = 7.4 Hz, 3H). ^{13}C NMR (151 MHz, $CDCl_3$) δ 163.64, 163.61, 133.19, 132.01, 131.20, 131.08, 130.62, 130.17, 129.01, 128.07, 123.16, 122.30, 77.24, 77.03, 76.82, 42.08, 21.37, 11.51.

Synthesis of Nap-PZ

Piperazine (0.855 g, 9.93 mmol) was dissolved in 2-methoxyethanol (15 mL), and compound 2 (0.79 g, 2.48 mmol) was added. The reaction mixture was stirred and refluxed for 4 h under nitrogen atmosphere. After cooling to room temperature, the solvent was evaporated under reduced pressure, and the crude product was purified by silica gel column chromatography using CH_2Cl_2/MeOH (25:1, v/v) as eluent to give yellow solid (0.6 g ; yield 74.72%).^{1}H NMR (600 MHz, MeOD) δ 8.40 (ddd, J = 6.6, 5.0, 0.9 Hz, 2H), 8.35 (d, J = 8.1 Hz, 1H), 7.68 (dd, J = 8.3, 7.3 Hz, 1H), 7.24 (d, J = 8.1 Hz, 1H), 4.06 – 4.00 (m, 2H), 3.24 (d, J = 4.8 Hz, 4H), 3.19 – 3.14 (m, 4H), 1.75 – 1.66 (m, 2H), 0.99 (t, J = 7.5 Hz, 3H). ^{13}C NMR (151 MHz, MeOD) δ 164.44, 164.05, 156.53, 132.29, 130.69, 130.45, 129.57, 125.99, 125.51, 122.70, 116.03, 114.81, 53.43, 48.03, 47.88, 47.74, 47.60, 47.46, 47.32, 47.17, 45.18, 41.31, 20.98, 10.33. HRMS calcd for $C_{19}H_{22}N_3O_2^{+}$ ([M + H] $^{+}$) 324.1706, found 324.1700.

Synthesis of compound 4

A mixture of compound **3** (0.261 g, 1.48 mmol), K_2CO_3 (0.256 g, 1.86 mmol) and **Nap-PZ** (0.4, 1.24 mmol) in 15 mL dry acetone was refluxed for **6** h, then cooled to room temperature,

filtered, and the filter-cake was washed with acetone for three times. The crude product from the concentration of the filtrate in vacuum was purified by silica gel column chromatography using CH_2Cl_2/MeOH (60:1, v/v) as eluent to afford yellow solid (0.43 g ; yield 83.07%). ^{1}H NMR (600 MHz, $CDCl_3$) δ 8.59 (dt, J = 5.7, 2.8 Hz, 1H), 8.53 (dd, J = 8.0, 5.7 Hz, 1H), 8.42 – 8.37 (m, 1H), 7.74 – 7.68 (m, 1H), 7.35 (s, 1H), 7.25 (dd, J = 8.0, 4.5 Hz, 1H), 4.18 – 4.10 (m, 4H), 3.34 (s, 4H), 3.23 (s, 2H), 2.91 (s, 4H), 2.27 (t, J = 2.5 Hz, 1H), 1.79 – 1.74 (m, 2H), 1.02 (td, J = 7.4, 3.2 Hz, 3H). ^{13}C NMR (151 MHz, $CDCl_3$) δ 169.58, 164.43, 164.00, 155.42, 132.38, 131.17, 129.98, 129.83, 126.20, 125.89, 123.37, 117.26, 115.07, 79.52, 71.53, 61.39, 53.62, 53.05, 41.81, 28.74, 21.43, 11.54.

Synthesis of Nap-OH

To a solution of 4 (0.25 g, 0.60 mmol) and 5 (63 mg, 0.72 mmol) in THF (4 mL) was added a solution of sodium ascorbate (48 mg, 0.24 mmol) and $CuSO_4 \cdot 5H_2O$ (48 mg, 0.19 mmol) in distilled H_2O (4 mL). The reaction mixture was stirred for 4 h at r.t. under argon. The solvent was evaporated under reduced pressure, and the crude product was purified by silica gel column chromatography using CH_2Cl_2/MeOH (10:1, v/v) as eluent to afford yellow solid (0.253 g; yield 83.77%). ^{1}H NMR (600 MHz, $CDCl_3$) δ 8.62 – 8.56 (m, 1H), 8.52 (d, J = 8.0 Hz, 1H), 8.38 (d, J = 8.4 Hz, 1H), 7.85 (t, J = 5.8 Hz, 1H), 7.72 (s, 1H), 7.72 – 7.68 (m, 1H), 7.23 (d, J = 8.0 Hz, 1H), 4.57 (d, J = 6.0 Hz, 2H), 4.52 – 4.47 (m, 2H), 4.17 – 4.11 (m, 2H), 4.10 – 4.05 (m, 2H), 3.32 (s, 4H), 3.20 (s, 2H), 2.87 (s, 4H), 1.81 – 1.72 (m, 2H), 1.02 (t, J = 7.4 Hz, 3H). ^{13}C NMR (151 MHz, $CDCl_3$) δ 170.36, 164.48, 164.03, 155.49, 144.40, 132.46, 131.14, 130.02, 129.83, 126.17, 125.82, 123.33, 123.31, 117.13, 115.12, 61.46, 61.07, 53.61, 52.99, 52.69, 41.82, 34.48, 21.42, 11.53. HRMS calcd for $C_{26}H_{32}N_7O_4^+$ ([M + H]$^+$) 506.2510, found 506.2503.

Synthesis of Nap-Glc

Nap-Glc was synthesized with similar procedures to **Nap-OH.**^{1}H NMR (600 MHz, CD_3OD) δ 8.37 (ddd, J = 31.1, 15.0, 7.7 Hz, 3H), 8.12 (s, 1H), 7.67 (dt, J = 14.2, 4.7 Hz, 1H), 7.23 (dd, J = 10.3, 5.2 Hz, 1H), 5.62 (d, J = 9.2 Hz, 1H), 4.57 (s, 2H), 4.03 (dd, J = 11.6, 6.1 Hz, 2H), 3.90 (dt, J = 12.3, 5.5 Hz, 2H), 3.72 (dd, J = 12.2, 5.5 Hz, 1H), 3.61 – 3.56 (m, 2H), 3.53 – 3.49 (m, 1H), 3.37 (s, 1H), 3.30 (s, 3H), 3.24 (s, 2H), 2.87 (s, 4H), 1.70 (dd, J = 13.7, 7.3 Hz, 2H), 0.99 (t, J = 7.3 Hz, 3H). ^{13}C NMR (151 MHz, CD_3OD) δ 171.49, 164.42, 164.02, 156.14, 144.83, 132.27, 130.68, 130.45, 129.50, 125.86, 125.47, 122.64, 122.04, 115.90, 114.81, 88.19, 79.73, 77.07, 72.63, 69.51, 60.99, 60.82, 53.41, 53.10, 52.58, 41.32, 33.97, 20.99, 10.36. HRMS calcd for $C_{30}H_{38}N_7O_8^+$ ([M + H] $^+$) 624.2776, found 624.2758.

Spectroscopic measurements

The stock solutions of 1 mM of $Fe(NO_3)_3 \cdot 9H_2O$, $Cu(NO_3)_2 \cdot 3H_2O$, $Pb(NO_3)_2$, $Eu(NO_3)_3 \cdot 6H_2O$, $Co(NO_3)_2 \cdot 6H_2O$, $Ce(NO_3)_3 \cdot 6H_2O$, $Cd(NO_3)_2 \cdot 4H_2O$, $AgNO_3$, $Ba(NO_3)_2$, $Ni(NO_3)_2 \cdot 6H_2O$, NH_4Cl, $ZnCl_2$, $CaCl_2$, $CaCl_2$, NaCl, KCl, $MgSO_4$, $FeSO_4 \cdot 7H_2O$, $MnSO_4 \cdot H_2O$, CH_3COONa, $NaHSO_3$, Na_2SO_3, NaF, NaBr, NaI, and $NaNO_3$, $Na_2HPO_4 \cdot 2H_2O$ were prepared in deionized water. The stock solution of probes (1 mM) was prepared in DMSO. The fluorescence was measured with an excitation wavelength at 405 nm by scanning the spectra between 350 nm and 680 nm. The bandwidth for both excitation and emission spectra was 3 nm.

Cytotoxicity assays

HepG2 cells were incubated overnight on 96-well plates in growth medium, and each well contained 5000 HepG2 cells. The cells were then treated with different concentrations of probes for 24 h. The medium was removed and 10μL of MTT (5 mg/mL) was added to the wells. After incubation of 4 h at 37 °C, the absorbance was recorded by an ELX800 absorbance microplate reader at 490 nm. The relative viabilities of cells were calculated based on the data of five parallel tests.

Computational details

The ground state geometries optimizations and exited state calculations were respectively performed at density functional theory (DFT) and time-dependent density functional theory (TD-DFT)[54] level with hybrid B3LYP[55, 56] functional using the polarized continuum (PCM)[57] solvation model. 6-31g (d, p) basis set was employed for the main group atoms (C, H, O, N), whereas lanl2dz basis set, an effective core potential basis set, was used for Fe with optimized secondary p function and additional f-polarization function (ζf=0.246)[58, 59]. Frequency calculation was carried out at the same level of theory to ensure the optimized structure was a minimum. TD-DFT calculations based on the corresponding optimized structure of the ground state were used to calculate the vertical excitation energies and interpret the absorption spectra (UV-vis spectrum) in solvent (water). To reveal the reason for "fluorescent on" phenomenon, further TD-DFT calculation on the first singlet excited state was also conducted on **Nap-Glc** to provide its excited state geometry as well as reproduce emission energies. The electronic transitions character was assigned based on the frontier molecular orbitals analysis. All calculations were carried out using the Gaussian 09 package[60].

Cell imaging assay

HepG2 cell lines were incubated for 24 h in DMEM medium (5% CO_2, 37°C) and then treated with probe **Nap-Glc** (10 μM) for 30 min, washed twice with PBS to remove the extracellular probe. The cells were fixed by 4% paraformaldehyde solution at room temperature and washed 4 times with deionized water, after that, the cells were treated with different concentrations of Fe^{3+} and incubated for 20 min. Finally, the cell images of HepG2 treated with **Nap-Glc** alone, **Nap-Glc** and different concentrations Fe^{3+} were taken with Multi-photon laser confocal scanning microscopy.

Acknowledgements

W. J. Y. thanks the support of the National Natural Science Foundation of China (No.21262004) and Guangxi Key Laboratory of Traditional Chinese Medicine Quality Standards (No.201602), and

W. M. thanks the support of Study Abroad Program for Excellent Ph.D Students of Guangxi Zhuang Autonomous Region.

References

1. S. Epsztejn, H. Glickstein, V. Picard, I. N. Slotki, W. Breuer, C. Beaumont and Z. I. Cabantchik, *Blood*, 1999, 94, 3593-3603.
2. N. Narayanaswamy and T. Govindaraju, *Sensor Actuat B-Chem*, 2012, 161, 304-310.
3. J. H. Xu, Y. M. Hou, Q. J. Ma, X. F. Wu and X. J. Wei, *SpectrochimActaA,* 2013, 112, 116-124.
4. J. R. Burdo and J. R. Connor, *BioMetals*, 2003, 16, 63.
5. D. J. Bonda, H. G. Lee, J. A. Blair, X. Zhu, G. Perry and M. A. Smith, *Metallomics*, 2011, 3, 267-270.
6. X. Bao, X. Cao, X. Nie, Y. Xu, W. Guo, B. Zhou, L. Zhang, H. Liao and T. Pang, *Sensor Actuat B-Chem*, 2015, 208, 54-66.
7. H. Chen, X. Bao, H. Shu, B. Zhou, R. Ye and J. Zhu, *Sensor Actuat B-Chem*, 2017, 242, 921-931.
8. M. H. Lee, T. V. Giap, S. H. Kim, Y. H. Lee, C. Kang and J. S. Kim, *Chem Commun (Camb)*, 2010, 46, 1407-1409.
9. C. Queirós, A. M. G. Silva, S. C. Lopes, G. Ivanova, P. Gameiro and M. Rangel, *Dyes Pigments*, 2012, 93, 1447-1455.
10. J. Nandre, S. Patil, V. Patil, F. Yu, L. Chen, S. Sahoo, T. Prior, C. Redshaw, P. Mahulikar and U. Patil, *Biosensbioelectron*, 2014, 61, 612-617.
11. L. Long, L. Zhou, L. Wang, S. Meng, A. Gong and C. Zhang, *Anal Chim Acta*, 2014, 812, 145-151.
12. N. R. Chereddy, M. V. Niladri Raju, P. Nagaraju, V. R. Krishnaswamy, P. S. Korrapati, P. R. Bangal and V. J. Rao, *Analyst*, 2014, 139, 6352-6356.
13. H. Zhu, J. Fan, B. Wang and X. Peng, *Chem Soc Rev*, 2015, 44, 4337-4366.
14. Z. Yan, L. Hu and J. You, *Anal. Methods*, 2016, 8, 5738-5754.
15. M. Saleem and K. H. Lee, *RSC Adv.*, 2015, 5, 72150-72287.
16. Z. Chen, X. Liang, H. Zhang, H. Xie, J. Liu, Y. Xu, W. Zhu, Y. Wang, X. Wang, S. Tan, D. Kuang and X. Qian, *J Med Chem*, 2010, 53, 2589-2600.
17. S. Banerjee, E. B. Veale, C. M. Phelan, S. A. Murphy, G. M. Tocci, L. J. Gillespie, D. O. Frimannsson, J. M. Kelly and T. Gunnlaugsson, *Chem Soc Rev*, 2013, 42, 1601-1618.
18. R. Jain, M. Mathur, S. Sikarwar and A. Mittal, *J Environ Manage*, 2007, 85, 956-964.
19. Jackson, R. K.; Shi, Y.; Yao, X.; Burdette, S. C. Dalton Trans 2010, 39, 4155.
20. Xu, L.; Xu, Y.; Zhu, W.; Yang, C.; Han, L.; Qian, X. Dalton Trans 2012, 41, 7212.
21. Wang, W.; Wen, Q.; Zhang, Y.; Fei, X.; Li, Y.; Yang, Q.; Xu, X. Dalton Trans 2013, 42, 1827.
22. Jia, J.; Wu, L.; Ding, Y.; Huang, C.; Zhu, W.; Xu, Y.; Qian, X. Dalton Trans 2016, 45, 9402.
23. C. B. Huang, H. R. Li, Y. Luo and L. Xu, *Dalton Trans*, 2014, 43, 8102-8108.
24. J. Liu and Y. Qian, *Dyes Pigments*, 2017, 136, 782-790.
25. J. F. Zhang, S. Kim, J. H. Han, S. J. Lee, T. Pradhan, Q. Y. Cao, C. Kang and J. S. Kim, *Org Lett*, 2011, 13, 5294-5297.
26. Y. Fu, J. Zhang, H. Wang, J.-L. Chen, P. Zhao, G.-R. Chen and X.-P. He, *Dyes Pigments*, 2016, 133, 372-379.
27. M. H. Lee, N. Park, C. Yi, J. H. Han, J. H. Hong, K. P. Kim, D. H. Kang, J. L. Sessler, C. Kang and J. S. Kim, *J Am Chem Soc*, 2014, 136, 14136-14142.
28. D. T. Shi, D. Zhou, Y. Zang, J. Li, G. R. Chen, T. D. James, X. P. He and H. Tian, *Chem Commun (Camb)*, 2015, 51, 3653-3655.
29. M. H. Lee, J. H. Han, P. S. Kwon, S. Bhuniya, J. Y. Kim, J. L. Sessler, C. Kang and J. S. Kim, *J Am Chem Soc*, 2012, 134, 1316-1322.
30. M. H. Lee, H. M. Jeon, J. H. Han, N. Park, C. Kang, J. L. Sessler and J. S. Kim, *J Am Chem Soc*, 2014, 136, 8430-8437.
31. P. Jin, C. Jiao, Z. Guo, Y. He, S. Zhu, H. Tian and W. Zhu, *ChemSci*, 2014, 5, 4012.
32. Y. Tang, X. Kong, A. Xu, B. Dong and W. Lin, *Angew Chem Int Ed Engl*, 2016, 55, 3356-3359.
33. M. H. Lee, J. H. Han, J. H. Lee, H. G. Choi, C. Kang and J. S. Kim, *J Am Chem Soc*, 2012, 134, 17314-17319.
34. Ryan, G. J.; Poynton, F. E.; Elmes, R. B.; Erby, M.; Williams, D. C.; Quinn, S. J.; Gunnlaugsson, T. Dalton Trans 2015, 44, 16332.
35. Z. Xu, K. H. Baek, H. N. Kim, J. Cui, X. Qian, D. R. Spring, I. Shin and J. Yoon, *J Am Chem Soc*, 2010, 132, 601.
36. L. Dong, Y. Zang, D. Zhou, X. P. He, G. R. Chen, T. D. James and J. Li, *Chem Commun (Camb)*, 2015, 51, 11852-11855.
37. *He, X. P.; Zeng, Y. L.; Tang, X. Y.; Li, N.; Zhou, D. M.; Chen, G. R.; Tian, H. Angew Chem Int Ed Engl 2016, 55, 13995.*
38. Li, K. B.; Zang, Y.; Wang, H.; Li, J.; Chen, G. R.; James, T. D.; He, X. P.; Tian, H. Chem Commun (Camb) 2014, 50, 11735.
39. He, X. P.; Zang, Y.; James, T. D.; Li, J.; Chen, G. R.; Xie, J. Chem Commun (Camb) 2017, 53, 82.
40. Xie, J.; Bogliotti, N. Chem Rev 2014, 114, 7678.
41. Hu, X.-L.; Zang, Y.; Li, J.; Chen, G.-R.; James, T. D.; He, X.-P.; Tian, H. Chem. Sci. 2016, 7, 4004.
42. Garcia, L.; Lazzaretti, M.; Diguet, A.; Mussi, F.; Bisceglie, F.; Xie, J.; Pelosi, G.; Buschini, A.; Baigl, D.; Policar, C. New Journal of Chemistry 2013, 37, 3030.
43. Burke, H. M.; Gunnlaugsson, T.; Scanlan, E. M. Chem Commun (Camb) 2015, 51, 10576.
44. Calatrava-Perez, E.; Bright, S. A.; Achermann, S.; Moylan, C.; Senge, M. O.; Veale, E. B.; Williams, D. C.; Gunnlaugsson, T.; Scanlan, E. M. Chem Commun (Camb) 2016, 52, 13086.
45. Burke, H. M.; Gunnlaugsson, T.; Scanlan, E. M. Organic & biomolecular chemistry 2016, 14, 9133.
46. J. Chen, Y. Li, K. Lv, W. Zhong, H. Wang, Z. Wu, P. Yi and J. Jiang, *Sensor Actuat B-Chem*, 2016, 224, 298-306.
47. S. Joshi, S. Kumari, R. Bhattacharjee, A. Sarmah, R. Sakhuja and D. D. Pant, *Sensor Actuat B-Chem*, 2015, 220, 1266-1278.
48. L.F. Zhang, J.L. Zhao, X. Zeng, L. Mu, X.K. Jiang, M. Deng, J.X. Zhang and G. Wei, *Sensor Actuat B-Chem*, 2011, 160, 662-669.
49. J. Liu and Y. Qian,*J Lumin*, 2017, 187, 33-39.
50. B. Sui, S. Tang, T. Liu, B. Kim and K. D. Belfield, *ACS Appl Mater Inter*, 2014, 6, 18408-18412.
51. S.R. Liu and S.P. Wu, *Sensor Actuat B-Chem*, 2012, 171-172, 1110-1116.
52. A. Mitra, B. Ramanujam and C. P. Rao, *Tetrahedron Lett*, 2009, 50, 776-780.
53. H. A. McIlwee, C. L. Schauer, V. G. Praig, R. Boukherroub and S. Szunerits, *Analyst*, 2008, 133, 673-677.

View Article Online
DOI: 10.1039/C7DT01099K

54. A. D. Laurent and D. Jacquemin, *Int J Quantum Chem*, 2013, 113, 2019-2039.
55. C. Lee, W. Yang and R. G. Parr, Phys Rev B, 1988, 37, 785-789.
56. A. D. Becke, *J Chem Phys*, 1993, 98, 5648-5652.
57. G. Scalmani and M. J. Frisch, *J Chem Phys*, 2010, 132, 114110.
58. M. Couty and M. B. Hall, *J Comput Chem*, 1996, 17, 1359-1370.
59. A. W. Ehlers, M. Böhme, S. Dapprich, A. Gobbi, A. Höllwarth, V. Jonas, K. F. Köhler, R. Stegmann, A. Veldkamp and G. Frenking, *Chem Phys Lett*, 1993, 208, 111–114.
60. M. J. Frisch, et al. Gaussian 09, revision C.01, Gaussian, Inc., Wallingford, CT, 2010.